

Research Article

Structure design and coordinated motion analysis of bionic crocodile robot

Jun Wang, Jingya Zheng, Yuhang Zhao, Kai Yang*

School of Information and Control Engineering, China University of Mining and Technology, Xuzhou 221116, China

ARTICLE INFO

Article history:

Received 30 October 2023

Revised 27 February 2024

Accepted 9 March 2024

Available online 20 March 2024

Keywords:

Bionic crocodile robot

Kinematic modeling

Motion simulation

Multipart coordination

ABSTRACT

Crocodiles, one of the oldest and most resilient species on Earth, have demonstrated remarkable locomotor abilities both on land and in water, evolving over millennia to adapt to diverse environments. In this study, we draw inspiration from crocodiles and design a highly biomimetic crocodile robot equipped with multiple degrees of freedom and articulated trunk joints. This design is based on comprehensive analysis of the structural and motion characteristics of real crocodiles. The bionic crocodile robot has a problem of limb-torso incoordination during movement. To solve this problem, we used the D-H method for both forward and inverse kinematics analysis of the robot's legs and spine. Through a series of simulation experiments, we investigated the robot's motion stability, fault tolerance, and adaptability to environments in two motor patterns: with and without spine and tail movements. The experimental results show that the bionic crocodile robot exhibits superior motion performance when the spine and tail cooperate with the extremities. This study not only demonstrates the potential of biomimicry in robotics but also underscores the significance of understanding how nature's designs can inform and enhance technological innovations.

© 2024 The Author(s). Published by Elsevier B.V. on behalf of Shandong University. This is an open access article under the CC BY-NC-ND license (<http://creativecommons.org/licenses/by-nc-nd/4.0/>).

1. Introduction

As technology continues to advance, robotics has become one of the most compelling fields in the world. In this rapidly developing field, legged robots, as mechanical systems with great potential and flexibility, have attracted extensive attention and research [1,2]. Their unique leg structure gives them the ability to adapt to complex terrain [3,4], enabling them to perform various tasks in different environments, showing great potential in areas such as exploration, search and rescue, manufacturing, and healthcare. Legged robots can be divided into two categories: legged walking and crawling robots. Legged crawling robots can choose their landing points in wider spaces and show better passability on complex terrain. In addition, the larger support polygon and lower center of gravity make legged robots more stable [5–8].

Crocodiles are highly evolved reptiles that can perform almost all quadrupedal gaits of mammals and have a powerful tail. The structural features of crocodiles [9] make them well-adapted to their environment. Their great adaptability to the environment is achieved through coordination between the legs and other parts of the body, such as the trunk, head, and tail. Crocodiles extend their stride length by bending their bodies and achieve balance by wagging their tails. These behaviors suggest that limb

coordination plays an important role in the control of biological locomotion [10–12], as crocodiles adapt to the environment through the coordination of multiple parts and allow a single part to perform multiple motion functions with the cooperation of other parts. However, there is still significant room for research on this limb-body coordination mechanism, and the study and improvement of this mechanism can help elucidate the motor control of crocodilians and be useful in the design of bionic crocodilian robots.

At present, there are few studies using alligators as robotic bionic objects worldwide. Kamilo Melo et al. used simple fabrication techniques and generic components to design and assemble a bionic crocodile robot, which was then tested in a real natural environment [13]. A bionic crocodile modular robot consisting of 14 small robot modules was designed at Ohio State University, USA, using an American alligator as a bionic object [14,15]. A low-cost open-source bionic crocodile robot platform was designed by a research team at the Indian Institute of Technology [16]. This platform allows rapid prototyping of robots and facilitates iterative design. Based on the bionic crocodile robot platform, the team investigated the effect of robot body torso swing on robot motion [17]; a research team at BITS Pilani (India) designed a new modular robot 2DxoPod by imitating the motion of vertebrates such as crocodiles and snakes [18]. This modular robot was designed with two mutually overlapping and orthogonal degrees of freedom to imitate the joints of creatures such as snakes, dogs, and crocodiles. The overall design was optimized by reducing

* Corresponding author.

E-mail address: yk267x@cumt.edu.cn (K. Yang).

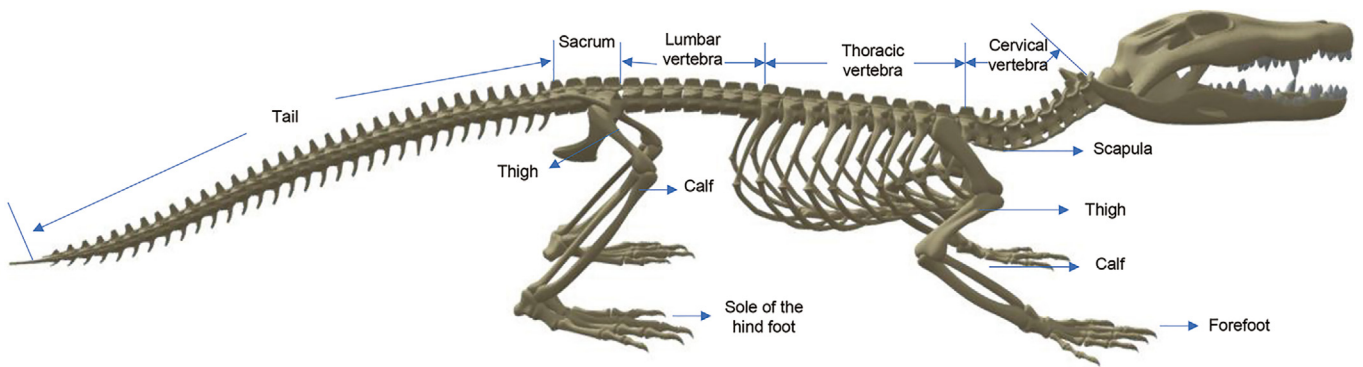


Fig. 1. Skeletal structure of the alligator.

the number of drives, degrees of freedom, and coordinates of the robot during navigation. However, none of these studies addressed the structural design of the crocodile spine and tail and their role in locomotion.

This study draws inspiration from the remarkable characteristics of crocodiles and applies them to the design of a bio-inspired crocodile robot. This study encompasses comprehensive structural analysis, a kinematic model established using the D-H method, and both forward and inverse kinematic analyses. This study focuses on achieving coordinated planning control among the various components of the bio-inspired crocodile by extracting the relationships between phases and angles of the limb, spine, and tail during a single motion cycle, closely mimicking the locomotion of real crocodiles. Subsequently, experimental analysis was performed to evaluate several key performance aspects of the bio-inspired crocodile robot. This evaluation includes an examination of its motion stability when subjected to coordinated planning control of the spine, limbs, and tail, an exploration of its resilience despite potential component damage, and an investigation into its adaptability in different environments.

Compared with other legged robots, the bionic crocodile robot designed in this study has not only legs but also a spine and tail, allowing it to perform more complex and flexible movements and even swim in water. Overall, this study not only highlights the potential of bio-inspired robotics but also provides insights into the robustness and adaptability of bio-inspired crocodile robots in various environments.

2. Structural design

2.1. Structure and movement characteristics of Crocodile

Crocodiles are remarkable semi-aquatic and semiterrestrial creatures that inhabit several regions across the world, spanning tropical, subtropical, and temperate areas in Asia, Africa, America, and Oceania. Globally, there are currently 26 recognized crocodile species, all belonging to the biological order Crocodylia [19–22]. Within the Crocodylia order, crocodiles are categorized into three major families: Alligatoridae, Crocodylidae, and Gavialidae. These diverse species exhibit a vast range of sizes, with the African Nile Crocodile being the largest among them, reaching an average length of approximately 4 m [23]. In contrast, the Chinese alligator (*Alligator sinensis*), a member of the Alligatoridae family, represents the smallest crocodile species, typically measuring approximately 1.25 m in length [24].

In this section, we analyze crocodiles within the Alligatoridae family, focusing on their structural characteristics. Fig. 1 illustrates the skeletal structure of Alligatoridae crocodiles.

An intriguing observation reveals that a crocodile's tail boasts a greater number of segments than its spine, with the tail length

accounting for approximately half of the crocodile's overall body length. Crocodiles' legs are short, with the scapula connecting the front two legs. The front legs exhibit five toes, the hind legs feature four toes, and the hind feet adopt a webbed structure.

Through continuous evolution, crocodiles have acquired exceptional mobility and adaptability, demonstrating peak performance in various modes of movement, whether in water or on land. Common locomotion patterns of crocodiles include belly crawling, high walking, galloping, swimming, and underwater rolling [25].

Belly crawling, the most frequently observed terrestrial locomotion mode, involves the crocodile's body remaining close to the ground with minimal movement. In this mode, the front and hind legs move in a diagonal gait, while the tail swings alternately from side to side, creating a leisurely pace for crocodile movement.

Conversely, crocodiles can be observed raising their legs upright beneath their bodies, with their feet pointing in a direction of moving forward. They move in a diagonal gait, and approximately half of their tail alternates swinging along the ground. This mode typically ranges in speed from 5 to 10 km/h.

In addition, crocodiles, with their impressive burst of power, are capable of galloping movements, which represent their fastest mode of locomotion and are typically employed when attempting to escape. In aquatic environments, crocodiles tightly press their limbs against their body's sides while using their tail to generate the primary thrust for swimming. The tail's swinging motion resembles a sine wave, and crocodiles use rapid tail swings to accelerate. During this movement, the body trunk exhibits wave-like undulations that resemble a sine curve [26].

2.2. Structural design

In this study, we selected the spectacled caiman, a member of the Alligator genus *Alligator*, as our research subject. The design of the bionic crocodile robot was inspired by the distinct morphological characteristics of these species. The robot comprises multiple components, including the head, body trunk, limbs, and tail, with each part consisting of interconnected joints. For a visual representation of the overall structure, refer to Fig. 2.

In this study, the torso of the bionic crocodile robot is designed according to the body structure and motion of a real crocodile [27]. As shown in Fig. 4, five degrees of freedom were set in the torso, including three degrees of freedom for the lateral movement of the spinal column and two degrees of freedom for the robot's pitch motion.

The leg structure of the bionic crocodile robot was developed by analyzing the leg skeleton structure and movement patterns [28] of real crocodiles. As shown in Fig. 3, three degrees of freedom were set in the leg, including two joints at the hip and

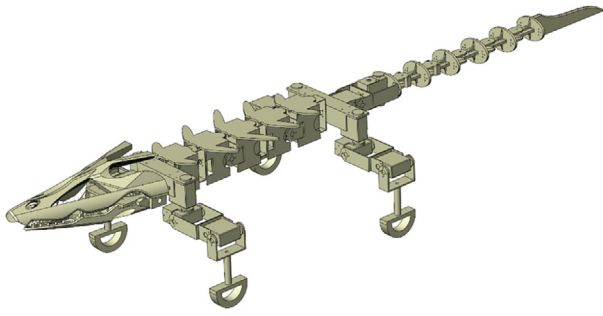


Fig. 2. Design of the overall structure of bionic crocodile robot.

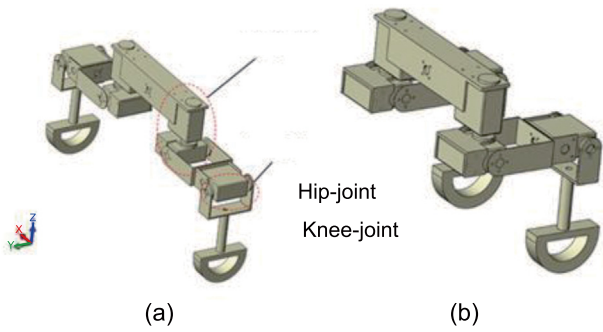


Fig. 3. Design of leg structure of bionic crocodile robot.

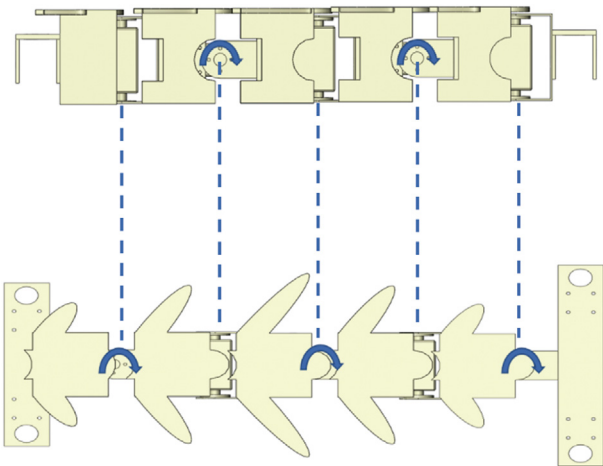


Fig. 4. Design of the torso of bionic crocodile robot.

one at the knee. When moving on a flat surface, the robot adopts the crawling structure illustrated in Fig. 3(a). Conversely, when traversing rough terrains, it uses the lactation-type structure shown in Fig. 3(b). This design allows the bionic crocodile robot to dynamically switch between different structures and gaits based on the environment encountered.

The design of the tail structure [29] of the crocodile robot is shown in Fig. 5. As depicted in Fig. 5, the tail of the bionic alligator robot consists of a drive section and an underdrive section, where the drive section has six degrees of freedom and moves with a

Table 1
D-H parameter table of rear limb.

i	θ_i (rad)	d_i (mm)	a_i (mm)	α_i (rad)
1	θ_1	0	70	0
2	θ_2	0	0	$\pi / 2$
3	θ_3	0	86	0
4	θ_4	0	89	0

linear drive. The underdrive section is made of flexible material, which can realistically simulate the flexible tail of an alligator.

We fabricate a physical prototype of a bionic crocodile robot that is driven by separate servos for each joint of the spine and limbs and a wire-driven tail, as shown in Fig. 6. The dimensions of the robot are 100*45*18 cm (length*width*height), and the weight is approximately 3.45 kg.

3. Kinematic analysis

The appropriate coordinate system is set for each joint to describe the correct kinematic characteristics of the bionic crocodile robot. In this study, the reference coordinate system [30] of the legs and spine of the bionic crocodile robot [31] was constructed using D-H representation, the homogeneous transformation matrix between the coordinate system of the robot's foot movement and the reference coordinate system of the base was obtained, and the relevant kinematic model was established.

3.1. Kinematic model of legs

Taking the left hind leg of a bionic crocodylian robot as an example, we establish the coordinate system of each rod and derive the corresponding kinematic equations using the D-H method. The D-H linkage coordinate system for the leg of the bionic crocodile robot according to the above steps is shown in Fig. 7.

According to the chain rule of coordinate system transformation, the flush transformation matrix of adjacent joint coordinate systems is expressed as follows:

$${}^{i-1}T_i = \begin{bmatrix} c\theta_i & -s\theta_i & 0 & a_{i-1} \\ s\theta_i c\alpha_{i-1} & c\theta_i c\alpha_{i-1} & -s\alpha_{i-1} & -s\alpha_{i-1}d_i \\ s\theta_i s\alpha_{i-1} & c\theta_i s\alpha_{i-1} & c\alpha_{i-1} & c\alpha_{i-1}d_i \\ 0 & 0 & 0 & 1 \end{bmatrix} \quad (1)$$

where $c(\cdot)$ and $s(\cdot)$ represent the cosine and sine of the angle, respectively.

Based on the established coordinate system of the bionic crocodile robot, its D-H parameters were determined, as listed in Table 1, where a_i , α_i , d_i , and θ_i denote the length of the connecting rod, angle of the connecting rod, deviation of the connecting rod, and joint angle, respectively.

The determined D-H parameters are inserted into Eq. (1) to obtain the position transformation matrix of each joint of the back leg of the bionic crocodile robot:

$${}^0T_1 = \begin{bmatrix} c\theta_1 & -s\theta_1 & 0 & a_1 \\ s\theta_1 & c\theta_1 & 0 & 0 \\ 0 & 0 & 1 & 0 \\ 0 & 0 & 0 & 1 \end{bmatrix} \quad (2)$$

$${}^1T_2 = \begin{bmatrix} c\theta_2 & -s\theta_2 & 0 & a_2 \\ 0 & 0 & -1 & 0 \\ s\theta_2 & c\theta_2 & 0 & 0 \\ 0 & 0 & 0 & 1 \end{bmatrix} \quad (3)$$

$${}^2T_3 = \begin{bmatrix} c\theta_3 & -s\theta_3 & 0 & a_3 \\ s\theta_3 & c\theta_3 & 0 & 0 \\ 0 & 0 & 1 & 0 \\ 0 & 0 & 0 & 1 \end{bmatrix} \quad (4)$$

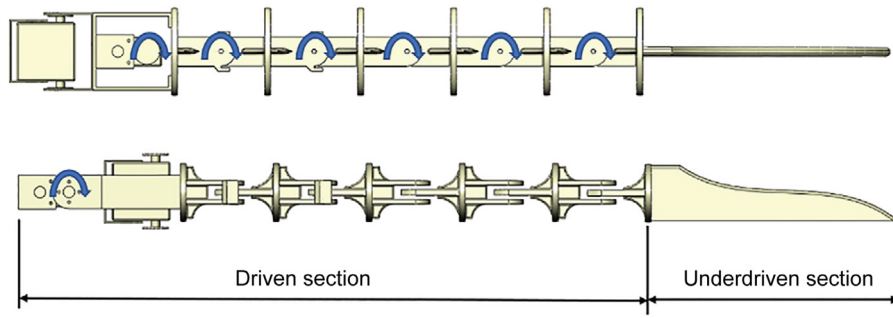


Fig. 5. Design of the tail of bionic crocodile robot.

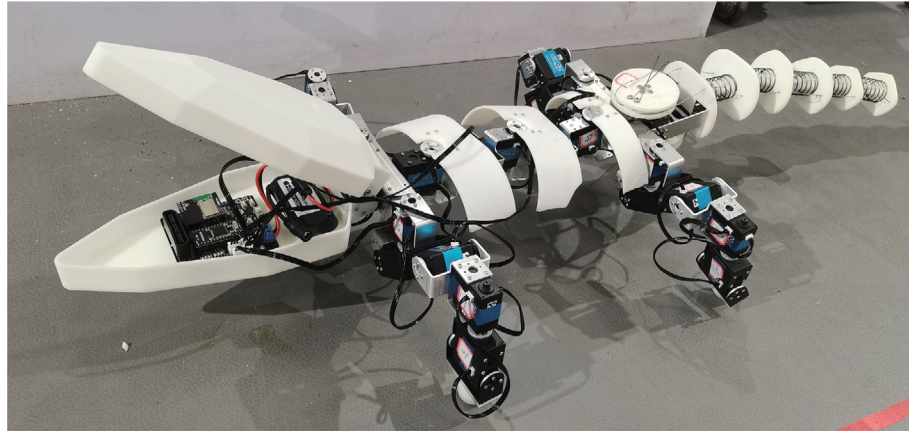


Fig. 6. Bionic crocodile robot prototype.

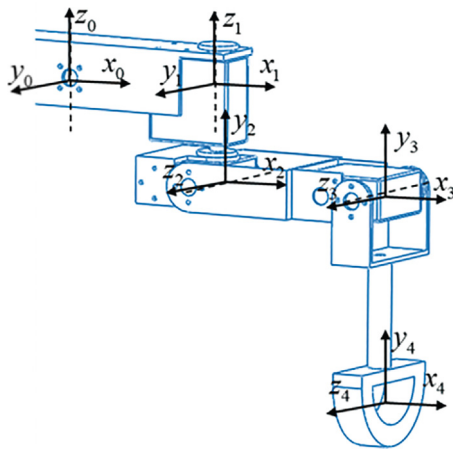


Fig. 7. D-H coordinate system of hind limb.

$${}^3T_4 = \begin{bmatrix} c\theta_4 & -s\theta_4 & 0 & a_4 \\ s\theta_4 & c\theta_4 & 0 & 0 \\ 0 & 0 & 1 & 0 \\ 0 & 0 & 0 & 1 \end{bmatrix} \quad (5)$$

After solving the matrix operation and sorting it out, we obtain

$${}^0T_4 = {}^0T_1 {}^1T_2 {}^2T_3 {}^3T_4 = \begin{bmatrix} n_x & o_x & a_x & p_x \\ n_y & o_y & a_y & p_y \\ n_z & o_z & a_z & p_z \\ 0 & 0 & 0 & 1 \end{bmatrix} \quad (6)$$

By inserting the parameters from Table 1 into Eq. (6), we obtain

$$\begin{cases} n_x = c\theta_1 c(\theta_2 + \theta_3 + \theta_4) \\ n_y = s\theta_1 c(\theta_2 + \theta_3 + \theta_4) \\ n_z = s(\theta_2 + \theta_3 + \theta_4) \\ o_x = -c\theta_1 s(\theta_2 + \theta_3 + \theta_4) \\ o_y = -s\theta_1 s(\theta_2 + \theta_3 + \theta_4) \\ o_z = c(\theta_2 + \theta_3 + \theta_4) \\ p_x = a_0 - a_3(c\theta_1 s\theta_2 s\theta_3 - c\theta_1 c\theta_2 c\theta_3) + a_2 c\theta_1 c\theta_2 \\ p_y = s\theta_1(a_3 c(\theta_2 + \theta_3) + a_2 c\theta_2) \\ p_z = a_3 s(\theta_2 + \theta_3) + a_2 s\theta_2 \end{cases} \quad (7)$$

To verify the accuracy of the leg kinematics of the developed bionic crocodile robot, the robot toolbox in MATLAB was used to establish a simulation model of the robot's leg, as shown in Fig. 8.

Inverse kinematics involves determining the angles of each joint based on the position and orientation of the end-effector. It serves as the foundation for motion planning and foot trajectory control in bio-inspired crocodile robots.

This study employs a geometric analysis method for inverse kinematic analysis. We solved θ_1^t by placing it in the X-Y plane of the leg diagram of the bionic crocodile robot established above. Fig. 9(a) illustrates a schematic of the hind leg mechanism of the bio-inspired crocodile robot in the X-Y plane.

Based on the D-H linkage coordinate system established above and the measured data in the three-dimensional diagram of the robot leg, it can be concluded that the leg linkage of the bionic amphibious crocodile robot $OA = a_0^t$. Through the trigonometric function relationship, we obtain

$$\begin{cases} AD = P_x - a_0^t \\ CD = P_y \end{cases} \quad (8)$$

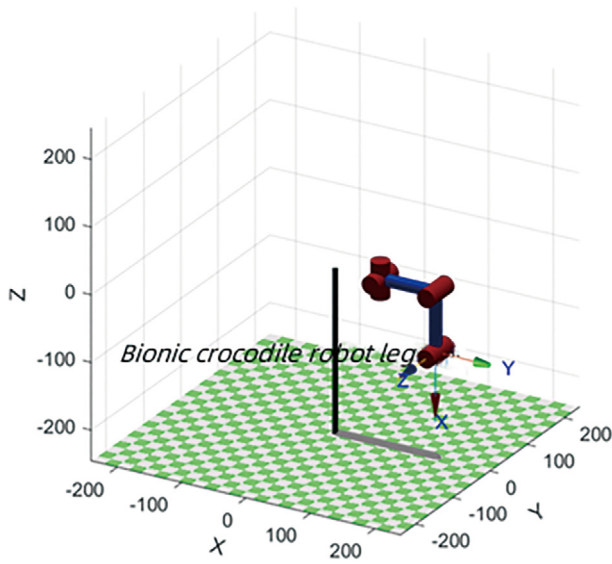


Fig. 8. Hind limb simulation mode.

Using Eq. (8), we derive the following:

$$\theta_1^t = \arctan \frac{P_y}{P_x - a_0^t} \quad (9)$$

A new coordinate system $X'-Z$ is established on the plane where point ABC is located, θ_2^t and θ_3^t are solved in the schematic of the legs of the bionic crocodile robot on the $X'-Z$ plane. As shown in Fig. 9(b), a schematic of the mechanism of the hind legs of the bionic amphibious crocodile robot in the $X'-Z$ plane is shown.

Through the D-H linkage coordinate system established above and the data measured by the three-dimensional diagram of the robot leg, it can be obtained that the leg linkage $AB = a_2^t$, the leg linkage $BC = a_3^t$, and the foot coordinate $(\sqrt{(P_x - a_0^t)^2 + P_y^2}, P_z)$, where point O represents the coordinate origin and θ_3^t denotes an outer angle of triangle ABC, which can be obtained using the following trigonometric function relationship:

$$\begin{cases} AB = a_2^t \\ BC = a_3^t \\ AC = \sqrt{(P_x - a_0^t)^2 + P_y^2 + P_z^2} \\ \angle ABC = \arccos \left[\frac{AB^2 + BC^2 - AC^2}{2AB \times BC} \right] \end{cases} \quad (10)$$

According to Eq. (10), Eqs. (11), (12), and (13) can be obtained as follows:

$$\begin{aligned} \theta_3^t &= 180^\circ - \angle ABC \\ &= 180^\circ - \arccos \left[\frac{a_2^{t2} + a_3^{t2} - ((P_x - a_0^t)^2 + P_y^2 + P_z^2)}{2a_2^t \times a_3^t} \right] \end{aligned} \quad (11)$$

$$\begin{cases} \angle CAZ = \arctan \left[\frac{\sqrt{(P_x - a_0^t)^2 + P_y^2}}{P_z} \right] \\ \angle CAB = \arccos \left[\frac{a_2^{t2} - a_3^{t2} + ((P_x - a_0^t)^2 + P_y^2 + P_z^2)}{2a_2^t \times \sqrt{(P_x - a_0^t)^2 + P_y^2 + P_z^2}} \right] \\ \theta_2^t = 90^\circ - \angle CAZ - \angle CAB \end{cases} \quad (12)$$

Table 2
D-H parameter of the torso.

i	θ_i (rad)	d_i (mm)	a_i (mm)	α_i (rad)
1	θ_1	0	50.5	0
2	θ_2	0	60.5	$-\pi / 2$
3	θ_3	0	60.5	$\pi / 2$
4	θ_4	0	60.5	$-\pi / 2$
5	θ_5	0	60.5	$\pi / 2$

$$\begin{aligned} \theta_2^t &= 90^\circ - \arctan \left[\frac{\sqrt{(P_x - a_0^t)^2 + P_y^2}}{P_z} \right] \\ &\quad - \arccos \left[\frac{a_2^{t2} - a_3^{t2} + ((P_x - a_0^t)^2 + P_y^2 + P_z^2)}{2a_2^t \times \sqrt{(P_x - a_0^t)^2 + P_y^2 + P_z^2}} \right] \end{aligned} \quad (13)$$

The inverse kinematic solution of the legs of the bionic crocodile robot is as follows:

$$\begin{cases} \theta_1^t = \arctan \frac{P_y}{P_x - a_0^t} \\ \theta_2^t = 90^\circ - \arctan \left[\frac{\sqrt{(P_x - a_0^t)^2 + P_y^2}}{P_z} \right] \\ \quad - \arccos \left[\frac{a_2^{t2} - a_3^{t2} + ((P_x - a_0^t)^2 + P_y^2 + P_z^2)}{2a_2^t \times \sqrt{(P_x - a_0^t)^2 + P_y^2 + P_z^2}} \right] \\ \theta_3^t = 180^\circ - \angle ABC = 180^\circ - \arccos \left[\frac{a_2^{t2} + a_3^{t2} - ((P_x - a_0^t)^2 + P_y^2 + P_z^2)}{2a_2^t \times a_3^t} \right] \\ \theta_4^t = \theta_4^t \end{cases} \quad (14)$$

3.2. Kinematic model of spine

The D-H linkage coordinate system of the spine of the bionic crocodile robot is shown in Fig. 10.

Based on the established D-H coordinate system of the torso, the D-H parameters were determined, as listed in Table 2. We obtain the position coordinates of the foot after solving the matrix operations and organizing them, as shown in Eq. (15):

$$\begin{cases} P_x = a_4(c\theta_1c\theta_2c\theta_3c\theta_4 - s\theta_1s\theta_3c\theta_4 - c\theta_1s\theta_2s\theta_4) \\ \quad + a_3(c\theta_1c\theta_2c\theta_3 - s\theta_1s\theta_3) + a_2c\theta_1c\theta_2 + a_1c\theta_1 + a_0 \\ P_y = a_4(s\theta_1c\theta_1c\theta_3c\theta_4 + c\theta_1s\theta_3c\theta_4 - s\theta_1s\theta_2s\theta_4) \\ \quad + a_3(s\theta_1c\theta_2c\theta_3 + c\theta_1s\theta_3) + a_2s\theta_1c\theta_2 + a_1s\theta_1 \\ P_z = -a_4(c\theta_3s\theta_2c\theta_4 + c\theta_2c\theta_4s\theta_4) - a_3s\theta_2c\theta_3 - a_2s\theta_2 \end{cases} \quad (15)$$

3.3. Analysis of flexible tail

The tail section of the developed bionic crocodile robot is shown in Fig. 11, which mainly comprises three parts: drive, line drive flexible, and underdrive section.

As shown in Fig. 11, the XOY coordinate system is set at the center of the joint plate between the drive and line drive (wire-driven) flexible parts. The wire-driven flexible part consists of six joints of equal length that are driven by a servo motor through a pair of inextensible wire cords of length L. When the servo motor rotates, one cord is elongated and the other is shortened, prompting the tail to bend.

The angle of curvature θ of the wire-driven flexible part is related to the length variation X of the wire rope, which is related to the angle of rotation ϕ of the servo motor.

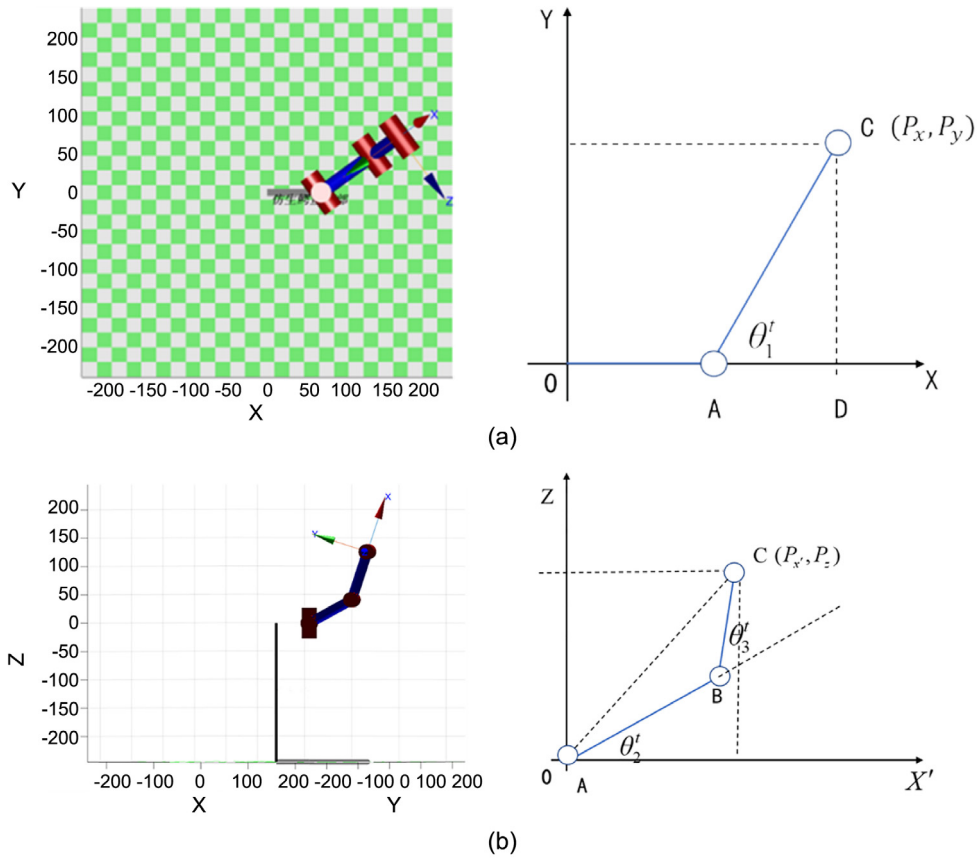


Fig. 9. Schematic diagram of kinematic analysis. (a) X-Y plane of hind limb. (b) Rear limb in X'-Z plane.

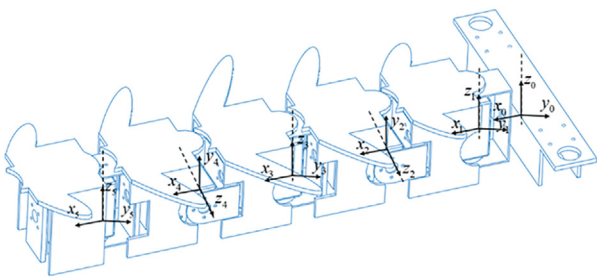


Fig. 10. D-H coordinate system of torso.

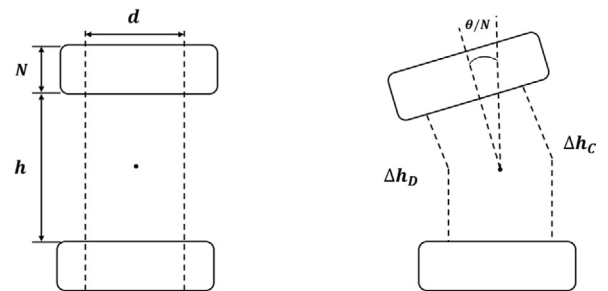


Fig. 12. Definition of tail parameters of bionic crocodile robot.

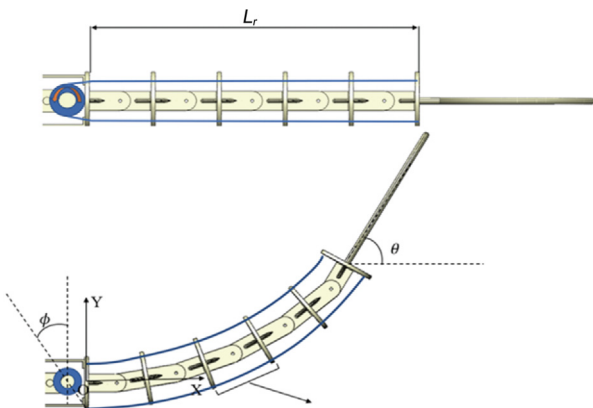


Fig. 11. Design of the flexible tail of bionic crocodile robot.

The angle of rotation of each joint is the same, and the change in the length of the two strings can be obtained as follows:

$$\begin{cases} \Delta h_D = - \left[ds \left(\frac{\theta}{2N} \right) + 2hs^2 \left(\frac{\theta}{4N} \right) \right] \\ \Delta h_C = ds \left(\frac{\theta}{2N} \right) - 2hs^2 \left(\frac{\theta}{4N} \right) \end{cases} \quad (16)$$

where N represents the number of joints, Δh_D denotes the length of the shortened cord, and Δh_C denotes the length of the extended cord. The definition of tail parameters for the bionic crocodile robot is shown in Fig. 12.

To simplify the calculation, the quadratic term in Eq. (16) can be ignored because the angle of rotation $\frac{\theta}{N}$ of each joint is

negligible.

$$\begin{cases} \Delta h_D = -ds(\frac{\theta}{2N}) \\ \Delta h_C = ds(\frac{\theta}{2N}) \end{cases} \quad (17)$$

The relationship between the angle of rotation of the servo motor and the length of the string extended or shortened is shown below, where r represents the radius of the steering wheel of the drive motor, ϕ denotes the rotation angle of the steering wheel, N represents the number of joints of the flexible tail, and θ denotes the final deviation angle of the flexible tail of the bionic crocodile robot.

$$\phi = \frac{180}{\pi r} N ds(\frac{\theta}{2N}) \quad (18)$$

The position of each joint in the XOY coordinate system can be expressed as follows:

$$\begin{cases} x_i = \begin{cases} \frac{H+h}{2}; i = 1 \\ \sum_{j=1}^{i-1} (H+h)c(\frac{j\theta}{N}); i \geq 2 \end{cases} \\ y_i = \begin{cases} 0; i = 1 \\ \sum_{j=1}^{i-1} (H+h)c(\frac{j\theta}{N}); i \geq 2 \end{cases} \end{cases} \quad (19)$$

where (x_i, y_i) denotes the position of the i th joint in the coordinate system XOY and N represents the number of active joints in the tail of the line drive.

3.4. Motion analysis of coordinated planning for multiple parts

Crocodiles exhibit an extraordinary degree of flexibility and adaptability in their natural environment, demonstrating remarkable freedom of movement. This exceptional mobility is achieved through coordinated cooperation of the limbs and other body parts, including the spine and tail. This underscores the critical role of synergy among these body components. Therefore, gaining a deeper understanding of the coordination mechanisms in crocodile locomotion is highly relevant for enhancing the motion control of bio-inspired crocodile robots.

By cultivating self-awareness in the limbs, spine, and tail and by closely observing the relative positions of these body parts during various movements such as crawling and jumping, we can achieve precise control over each component of the bio-inspired crocodile. Simultaneously, we can effectively coordinate the control of interactions among these components.

We established three feedback rules using self-perception feedback to achieve closed-loop control for individual components. These rules are as follows:

- (1) Limb-to-limb perception feedback.
- (2) Spine-to-spine perception feedback.
- (3) Tail-to-tail perception feedback.

Using these three rules, we can achieve stable closed-loop control of the limbs, spine, and tail of the bio-inspired crocodile robot. While the controllers for the limbs, spine, and tail operate independently, they are not isolated; they share certain variables (such as limb phase, spine bending angles and directions, and tail bending angles and directions) to ensure overall temporal and spatial coordination.

Fig. 13 presents a topological model established on the basis of biomechanical analysis of crocodile movements. In the model, we have incorporated foot-end pressure sensors and self-torque and position feedback sensors for the servo motors. We employed proportional-integral-derivative controllers for closed-loop control of the joint angles in the bio-inspired crocodile. The robot's

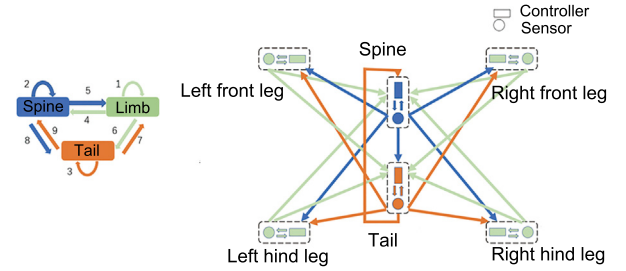


Fig. 13. Topological model.

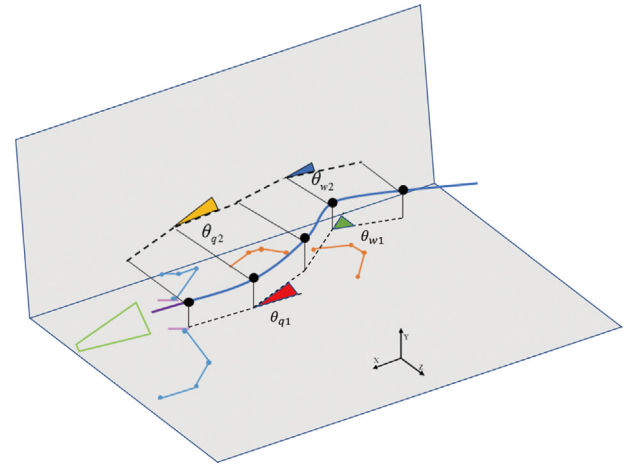


Fig. 14. Definition of angle and direction of crocodile spine and tail.

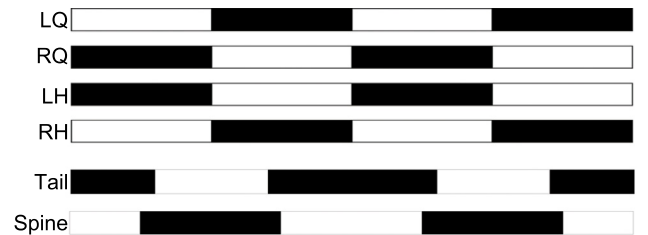


Fig. 15. Correspondence between the angle of the spine, the angle of the tail, and the phase of the gait.

leg section comprises one yaw joint servo motor, two pitch joint servo motors, and a joint angle controller. The spine section includes three yaw joint servo motors, two pitch joint servo motors, and a joint angle controller. The tail joint section comprises a pitch joint servo motor, a linear actuator for tail movement, and a joint angle controller. The joint angle controller is responsible for outputting the angle θ_i for each driver, where θ_i represents the target angle for each joint. In the target angle function, i represents the driver motor for each joint.

The video of the crocodile's movement was decomposed into continuous three-dimensional snapshots using ScreenToGif software. The relationship between the angle of the spine, the angle of the tail, and the phase of the crocodile's limbs was explored to link the various parts of the crocodile's body. The definitions of the angles of the spine and tail are shown in Fig. 14.

The black dots in Fig. 14 indicate the points used to calculate the angles, and the corresponding line segments are indicated by black dashed lines. The angles are shown as red and green

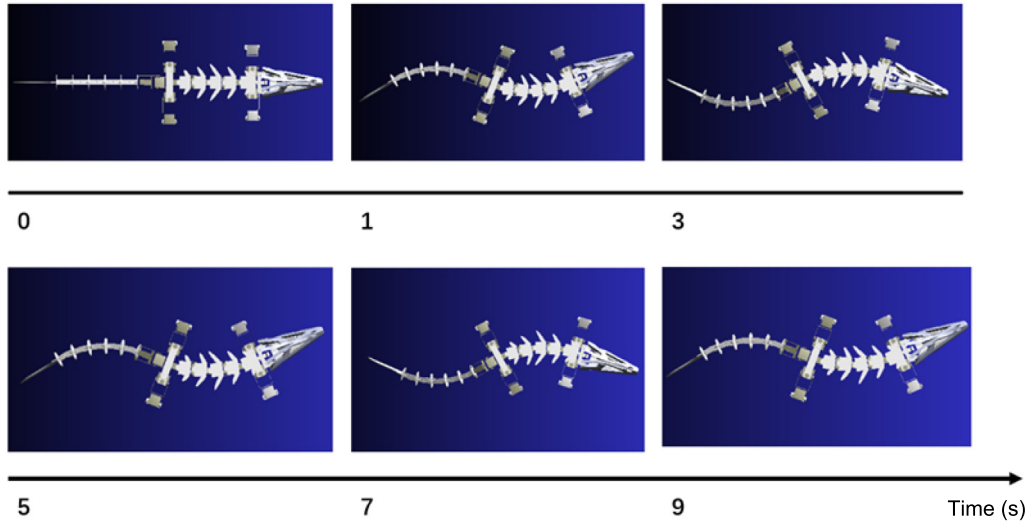


Fig. 16. Crawling process of bionic crocodile robot.

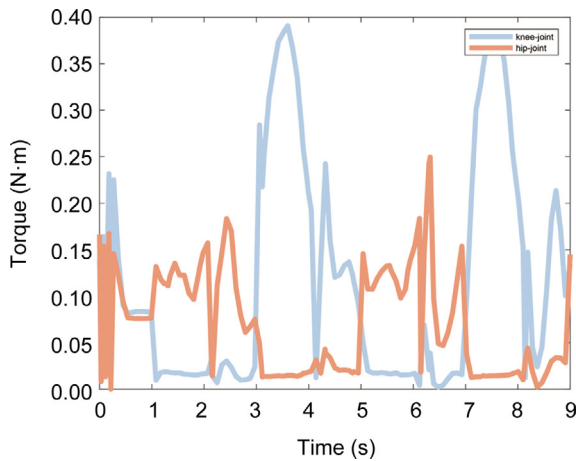


Fig. 17. Joint torque of bionic crocodile robot.

triangular areas (for pitch angles in the X-Z plane) and yellow and blue triangular areas (for yaw angles in the X-Y plane). Here, θ_{q1} indicates the pitch angle of the spine of the bionic crocodile robot. The angle is defined as negative when the spine is bent to the left side of the crocodile robot body and positive when the spine is bent to the right side of the robot body. θ_{w1} is defined as the pitch angle of the tail of the robot, which is defined as negative when the tail is bent to the left of the robot body. θ_{q2} is defined as the yaw angle of the spine of the robot, which is defined as negative when the spine is bent toward the top of the robot's body. θ_{w2} is defined as the yaw angle of the robot tail, which is defined as negative when the tail is bent to the top of the robot body and positive when the tail is bent to the bottom of the robot body.

As an example of the crocodilian crawl movement, the corresponding relationship between the angle of the spine joint, the angle of the tail joint, and gait in two cycles was extracted and obtained by the above procedure, as shown in Fig. 15. In the figure, the black area in the limb phase represents the landing phase, and the black area in the plots of the tail and spine represents the positive angle. LQ, RQ, LH, and RH refer to the left front leg, right front leg, left hind leg, and right hind leg, respectively.

4. Results

4.1. Standard walking experiment

First, we conducted a standard walking experiment in which the spine, legs, and tail of the bionic crocodile robot were involved in the movement and the robot walked in a diagonal gait on the plane. The experimental procedure is shown in Fig. 16.

When walking on the ground, the moments on the robot's leg joints are significantly larger than those on the spine and tail joints; therefore, we focus on analyzing the moments on the leg joints. In the simulation experiment, the mass of the robot was 3.5 kg, which is close to that of the physical prototype. Moments on the two leg joints are shown in Fig. 17. As shown in the figure, the knee joint is subjected to a greater moment than the hip joint, with a maximum moment of approximately 0.4 Nm, which is less than the rated moment of our servo.

4.2. Motion stability

Two groups of bionic crocodile robots were simulated or tested to determine whether coordinated movement of all parts of the bionic crocodile robot could improve its stability of motion. One group of bionic crocodile robots was set up to crawl with their limbs, tail, and spine, i.e., the tail dragged on the ground and the tail and spine swung left and right, whereas the other group of robots only crawled with their limbs, with the tail lifted off the ground and the spine and tail fixed.

Changes in the center of gravity of the two groups of bionic crocodile robots were recorded. The simulation experiment of the bionic crocodile robot is shown in Fig. 16. The experiment contains two complete crawling cycles, where 1–5 s is the first crawling cycle and 5–9 s is the second crawling cycle.

The state of the bionic crocodile robot during the crawling period was observed at three selected time points within a complete crawling cycle, as shown in Fig. 18, which are screenshots of the simulation experiments at 1.2, 1.5, and 1.8 s.

The upper part of Fig. 18 shows the motion state of the bionic crocodile robot with the participation of the tail, body, and limbs, and it crawls forward with a diagonal gait [32,33]. During the motion of the robot, the spine swings from side to side in a sinusoidal pattern with the limbs, and the tail stays on the ground

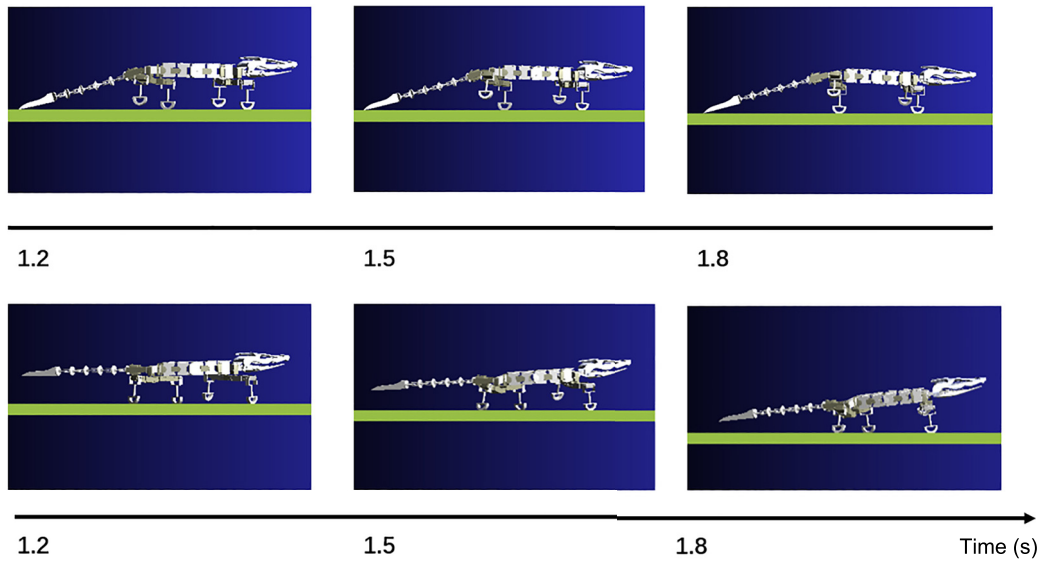


Fig. 18. Comparison of the stability of bionic crocodile robot during crawling.

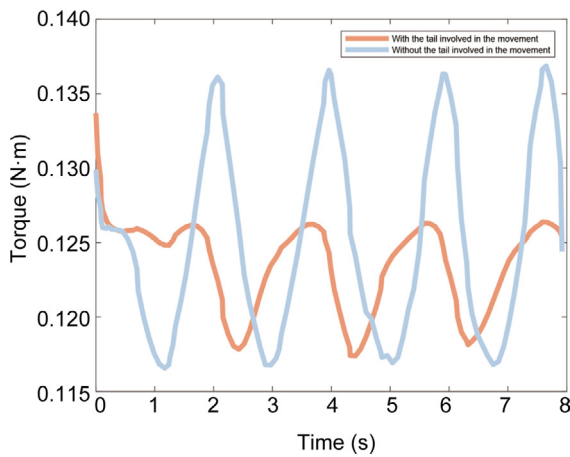


Fig. 19. Comparison of the fluctuation of the center of gravity between cases with and without tail movement.

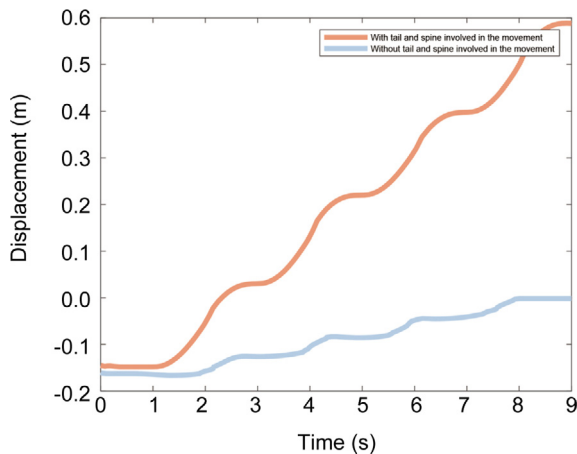


Fig. 20. Displacement with and without spine and tail movements.

and swings from side to side to provide support for the body and improve its stability. The bottom of Fig. 18 shows the crawling

state when the tail and spine are not involved in motion. When the robot's tail is not involved in the movement and it moves in a diagonal gait, the two legs on the ground simultaneously support and drive the body forward. The center of gravity should always be on the line of the two supporting points to achieve stability. The simulation experiment shows that at 1.2 s, the bionic crocodile robot tilts its body because the center of gravity is not on the line of the support points, and the robot shifts toward the center of gravity.

Fig. 19 shows the change in the height of the center of gravity during the movement of the two groups of bionic crocodile robots. Orange and blue represent the change in the height of the center of gravity with and without tail movement, respectively. From the figure, we observe that the change in the height of the center of gravity of the bionic crocodile robot varies in a certain way in both simulation experiments; however, the variation amplitude of the set with tail movement is significantly smaller than that of the set without tail movement, showing that the involvement of the tail in the movement of the bionic crocodile robot makes it more stable.

4.3. Crawling speed

To study the crawling speed of a bionic crocodile robot with or without tail and spine motion, the corresponding land motion and underwater motion simulation experiments were established.

The displacement of the two groups of robots moving on land is shown in Fig. 20. Fig. 20 shows the forward displacement of the bionic crocodile robot. The orange and blue curves represent displacement with or without spine and tail movement, respectively. The results indicate that within the same simulation time, the robot's forward displacement is 0.16 m when the spine and tail are not involved in the motion. However, when the spine, tail, and limbs are simultaneously involved in the motion, the robot achieves a displacement of 0.73 m in the forward direction. This comparison demonstrates that with spine and tail movements, the robot attains a higher velocity and covers a greater distance.

Upon observing the swimming behavior of real crocodiles in the water, it becomes evident that the primary forward thrust generated during crocodile swimming is achieved through the coordinated movement of the crocodile's body and the powerful action of its tail. To verify the role of the crocodile's spine and

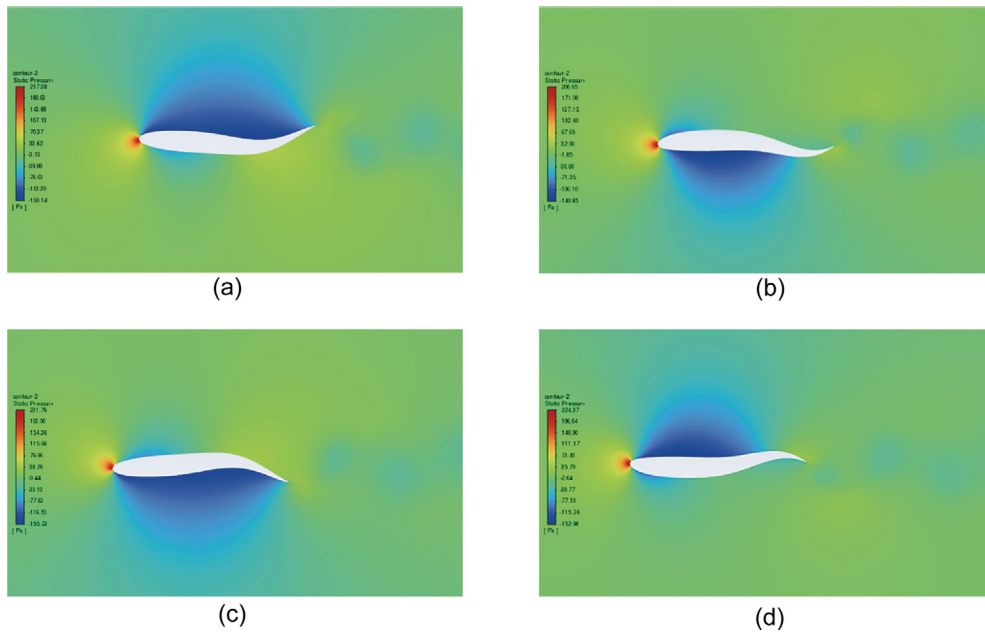


Fig. 21. Pressure nephogram of bionic crocodile robot in one swimming cycle. (a) $t = T/4$. (b) $t = T/2$. (c) $t = 3T/4$. (d) $t = T$.

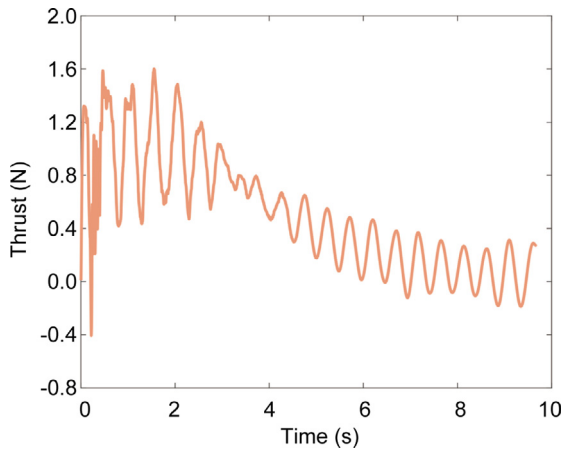


Fig. 22. Force on the bionic crocodile robot.

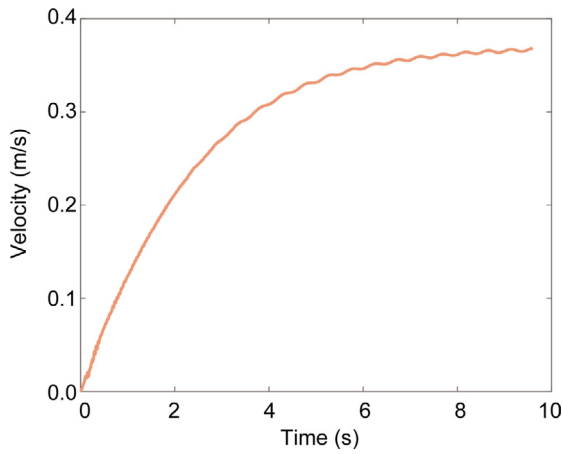


Fig. 23. Swimming speed of the bionic crocodile robot.

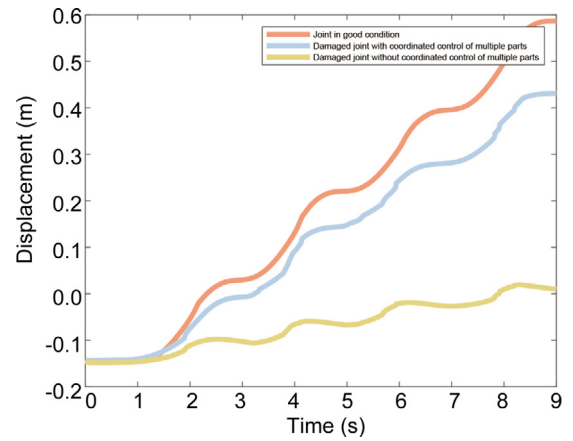


Fig. 24. Displacement of different bionic crocodile robots in the absence of rotating joints of the front leg.

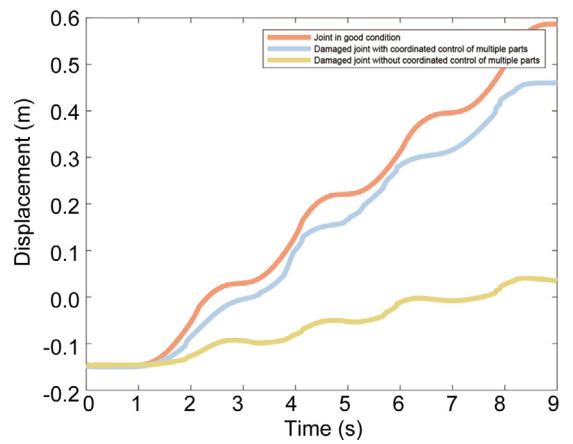


Fig. 25. Displacement of different bionic crocodile robots in the absence of rotating joints of the hind leg.

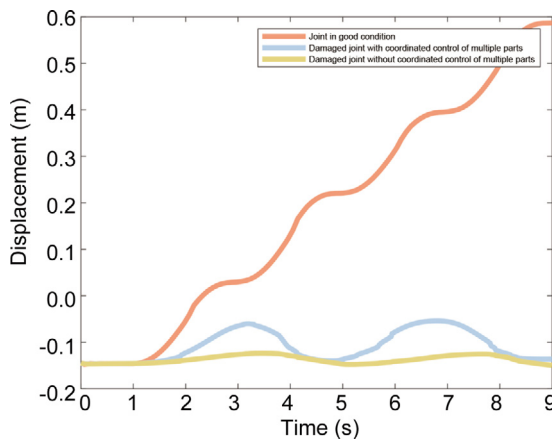


Fig. 26. Displacement of different bionic crocodile robots in the absence of pitching joint of front leg.

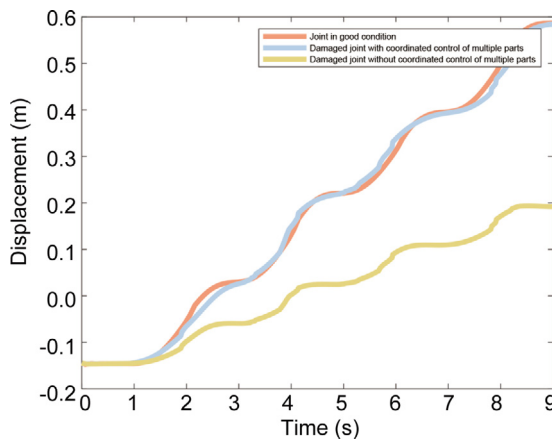


Fig. 27. Displacement of different bionic crocodile robots in the absence of pitching joint of hind leg.

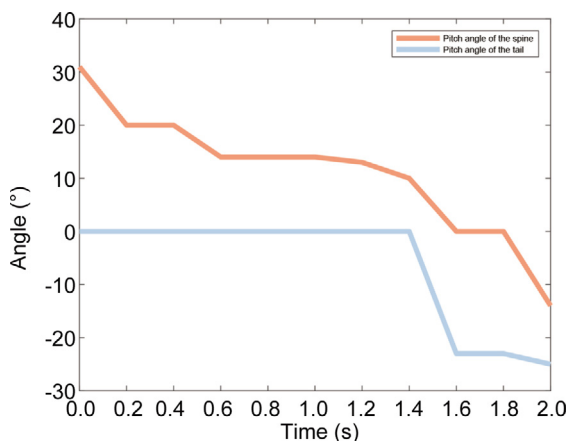


Fig. 28. Changes in the angle of the spine and tail of crocodile standing on two legs.

tail during aquatic locomotion, FLUENT software was employed to analyze the swimming dynamics of the bionic crocodile.

The swimming pattern of crocodiles in water closely resembles that of fish. Consequently, the body and tail movements of crocodiles are described in this study as fish-like body waves. The fish-like body wave curve is represented as a combination of the amplitude envelope of the fish body and a sine curve. The

mathematical function for the fish-like body wave is as follows:

$$y_{body}(x, t) = (c_1x + c_2x^2)s(kx + \omega t) \tag{20}$$

By measuring the center line parameters of the bionic crocodile robot, the center line trajectory is drawn and modeled in the form of a fish-like body wave function. The parameters of the fish-like body wave curve are $c_1=0.027$, $c_2=0.30$, and $k=0.023$.

Because crocodiles predominantly employ trunk and tail movements for propulsion during swimming, this study simplifies the bionic crocodile model by omitting the limbs and focusing on a two-dimensional body for simulation analysis.

Fig. 21 shows the pressure distribution during the swimming motion of the bionic crocodile robot. Fig. 21(a) displays the pressure distribution at T/4. The pressure on the bending and convex sides of the flexible tail is greater than that on the concave side. This pressure differential between the two sides of the flexible tail results in a diagonal forward force, propelling the robot in a diagonal direction. As the robot's body and tail continue their movement toward the head-to-tail axis, the pressure difference gradually decreases, as shown in Fig. 21(c). When the bionic crocodile's torso and tail reach 3T/4, the pressure difference between the two sides of the flexible tail generates a symmetrical diagonal forward thrust, producing an "S"-shaped swimming trajectory that closely resembles the natural swimming motion of real crocodiles.

To display specific information about the bionic crocodile robot when it moves forward in water more intuitively, the position and speed of the bionic crocodile robot's center of mass are solved using UDF (User-defined functions) of FLUENT.

Figs. 22 and 23 show the longitudinal external force and longitudinal motion velocity of the bionic crocodile robot, respectively, with a swinging motion period of 1 s.

In the 0–3 s stage, the combined force on the robot is large, and after the third second, the combined force gradually decreases and shows regular fluctuations. The speed of the robot first increases rapidly and then gradually stabilizes.

Two sets of experiments show that when the bionic crocodile robot moves on land, the swing of the tail and spine can improve the motion displacement. When moving through water, the swing of the tail and spine provides the main thrust.

4.4. Motion fault tolerance

To investigate the fault tolerance of the bionic crocodile robot in the coordinated movement of multiple parts, we assumed the paralysis of the leg in the experiment and compared its fault tolerance rate. Joint damage indicates that the actuator of the joint is unable to receive and execute motion commands. Here, four sets of comparative tests are set up to study the fault tolerance of the bionic crocodile robot when the front leg rotational joint, rear leg rotational joint, front leg pitching joint, and rear leg pitching joint are paralyzed.

Fig. 24 shows the displacement with and without the involvement of the spine in the case of a damaged rotating joint of the front leg. As shown in the figure, compared with the robot with intact joints and under coordinated control of multiple parts, the robot with damaged rotating joints of the front leg and without trunk cooperative motion has an 80% reduction in locomotion, and the robot with damaged front leg rotating joints but with trunk cooperative motion has only a 22% reduction in locomotion.

Fig. 25 shows the displacement with and without spine movement in the case of a damaged hind leg rotational joint. As shown in the figure, compared with the robot with intact joints and under coordinated control of multiple parts, the robot with a damaged hind leg rotating joint and without trunk cooperative motion has a 75% decrease in locomotion, whereas the robot with

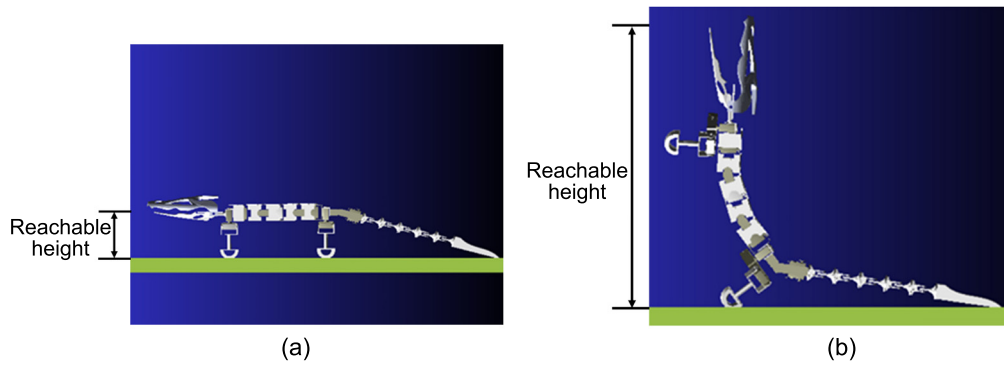


Fig. 29. Bionic crocodile robot stands bipedally. (a) State of crawling. (b) State of bipedal standing.

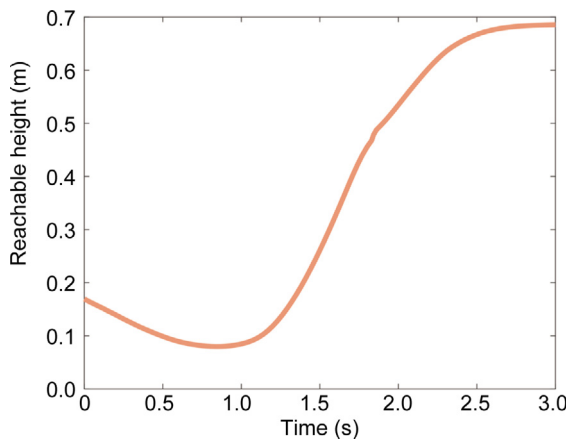


Fig. 30. Variation in reachable height for bipedal standing of bionic crocodile robot.

a damaged hind leg rotating joint but with trunk cooperative motion has only a 17% decrease in locomotion.

Fig. 26 shows the displacement with and without the involvement of the spine in the case of damage to the pitching joint of the front leg. As shown in the figure, damage to the pitching joint of the front leg caused the bionic crocodile robot to lose the ability to move forward.

Fig. 27 shows the displacement with and without spine movement for a damaged pitching joint of the hind leg. As shown in the figure, when the hind legs of the robot are missing, the bionic crocodile robot coordinated by multiple parts raises the center of gravity of the robot through the support function of the tail, right front leg, and left back leg so that the hind legs can be lifted off the ground and swing. Moreover, the ground where the robot moves is flat and does not require excessive step height; thus, the absence of a pitching joint of the hind legs can be overcome through coordinated control of multiple parts. The robot with a damaged pitching joint of the hind legs and without cooperating motion of the trunk had a 55% reduction in locomotion velocity due to the lack of torso coordination. In contrast, the robot with a damaged pitching joint of the hind legs and with cooperating motion of the trunk showed almost no reduction in locomotion compared with the robot with an intact joint.

4.5. Motion adaptability

As vertebrate reptiles, crocodiles have a low center of gravity when crawling on land, short legs, and low reachable heights. However, crocodiles are more adaptable to the external environment, and they can use their strong legs and powerful tails to

achieve a semi-standing posture, which increases their reachable height and facilitates their predation of prey at high places. To ensure that the movements of the crocodile robot were as close as possible to those of a real crocodile, we extracted the process of changes in the spine and tail joints during the transition from a quadrupedal to a bipedal stance from a real crocodile. The results are shown in Fig. 28.

Fig. 29 shows the side view of the bionic crocodile robot in the crawling and bipedal standing states. As shown in the figure, the reachable height of the bionic crocodile robot depends on the length of its legs when crawling on land. When the bionic crocodile robot stands through the biped and tail with the cooperation of the spine, tail, and hind limbs, the reachable height is determined by the length of the spine, head, and hind legs.

Fig. 30 shows the change in the height that the bionic crocodile robot can reach during the transition from the quadruped to biped standing states. As shown in the figure, the bionic crocodile robot can reach a height of 0.16 m in the crawling state and 0.68 m in the bipedal standing state. The reachable height in the bipedal standing state is 4.25 times higher than that in the crawling state.

The experiments show that the reachable height of the bionic crocodile robot is limited by leg length constraints when crawling on land. The coordination between the tail, spine, and hind limbs can improve the reachable height of the crocodile robot; thus, the working space of the crocodile robot can be significantly improved, and its adaptability to the environment can be enhanced.

5. Conclusion

In this study, we focus on a bionic crocodile robot using crocodiles as our biological model. First, we designed the structure of the bionic crocodile robot based on the morphological features and motion characteristics of real crocodiles. We employed the D-H method to establish kinematic models for the robot's legs and spine. Subsequently, we performed experimental analyses to evaluate the motion stability of the bionic crocodile robot under coordinated control of its spine, tail, and limbs, assessing its robustness despite potential damage and its ability to adapt to varying environments.

The results of our simulation experiments indicate that involving the spine and tail in conjunction with the limbs improves the stability of the bionic crocodile robot during movement. This combination results in increased displacement, heightened fault tolerance when individual joints are compromised, and improved adaptability to different environmental conditions. Consequently, we can deduce that limb coordination plays a pivotal role in animal locomotion.

On the basis of our theoretical analysis and the outcomes of the simulation experiments, we verified that the designed

bionic crocodile robot can attain a larger range of motion and fulfill a broader spectrum of functions when its components work together in a coordinated manner.

In our future work, we will focus on the bionic crocodile robot prototype to explore its amphibious locomotion performance on land and in water and its practical applications.

Declaration of competing interest

The authors declare that they have no known competing financial interests or personal relationships that could have appeared to influence the work reported in this paper.

Acknowledgment

This work was supported by the Graduate Research and Innovation Projects of Jiangsu Province (KYCX21_2251).

Appendix A. Supplementary data

Supplementary material related to this article can be found online at <https://doi.org/10.1016/j.birob.2024.100157>.

References

- [1] G. Bledt, M.J. Powell, B. Katz, et al., Mit cheetah 3: design and control of a robust, dynamic quadruped robot 2018, in: IEEE/RSJ International Conference on Intelligent Robots and Systems, IROS, IEEE, 2018, 22452252.
- [2] D. Dholakiya, S. Bhattacharya, A. Gunalan, et al., Design, development and experimental realization of a quadrupedal research platform: Stoch, in: 2019 5th International Conference on Control, Automation and Robotics, ICCAR, IEEE, 2019, pp. 229–234.
- [3] J. Lee, J. Hwangbo, L. Wellhausen, V. Koltun, M. Hutter, Learning quadrupedal locomotion over challenging terrain, *Science Robotics* 5 (47) (2020) eabc5986.
- [4] A. Kumar, Z. Fu, D. Pathak, et al., Rma: rapid motor adaptation for legged robots, 2021, arXiv preprint arXiv:2107.04034.
- [5] C. Zhiyuan, T.U. Qunzhang, Z. Xiangpo, et al., Review of multi-legged crawling robot, *J. Ordnance Equip. Eng.* 41 (09) (2020) 1–12.
- [6] S. Kitano, S. Hirose, A. Horigome, et al., TITAN-XIII: sprawling-type quadruped robot with ability of fast and energy-efficient walking, *Robomech J.* 3 (2016) 1–16.
- [7] P. Čížek, M. Zoula, Faigl J., Design, construction, and rough-terrain locomotion control of novel hexapod walking robot with four degrees of freedom per leg, *IEEE Access* 9 (2021) 17866–17881.
- [8] P.M. James, A. Prakash, V. Kalburgi, Sreedharan P., Design, analysis, manufacturing of four-legged walking robot with insect type leg, *Mater. Today: Proc.* 46 (2021) 4647–4652.
- [9] F. Akira, G. Megu, M. Yoichi, Comparative anatomy of quadruped robots and animals: a review, *Adv. Robot.* 36 (13) (2022).
- [10] D. Owaki, A. Ishiguro, A quadruped robot exhibiting spontaneous gait transitions from walking to trotting to galloping, *Sci. Rep.* 7 (2017) (2017) 277.
- [11] M. Hildebr, Motions of the running cheetah and horse, *J. Mammal.* 40 (4) (1959) 481–495.
- [12] K. Jagnandan, T.E. Higham, Lateral movements of a massive tail influence gecko locomotion: an integrative study comparing tail restriction and autotomy, *Sci. Rep.* 7 (2017) (2017) 10865.
- [13] K. Melo, T. Horvat, A.J. Ijspeert, Animal robots in the african wilderness: lessons learned and outlook for field robotics, *Science Robotics* 8 (85) (2023) eadd8662.
- [14] X. Jia, Z. Chen, J.M. Petrosino, et al., Biological undulation inspired swimming robot, in: 2017 IEEE International Conference on Robotics and Automation, ICRA, IEEE, 2017, pp. 4795–4800.
- [15] X. Jia, Z. Chen, J.M. Petrosino, et al., Biological undulation inspired swimming robot, in: 2017 IEEE International Conference on Robotics and Automation, ICRA, IEEE, 2017, pp. 4795–4800.
- [16] K.G. Karwa, S. Mondal, A. Kumar, et al., An open source low-cost alligator inspired robotic research platform, in: 2016 Sixth International Symposium on Embedded Computing and System Design, ISED, IEEE, 2016, 234238.
- [17] K. Agrawal, K. Jain, D. Gupta, et al., Bayesian optimization based terrestrial gait tuning for a 12-dof alligator-inspired robot with active body undulation, in: International Design Engineering Technical Conferences and Computers and Information in Engineering Conference, 2018, 51807: V05AT07A076.
- [18] R. Godiyal, T. Zodge, T. Rane, 2DxoPod-a modular robot for mimicking locomotion in vertebrates, *J. Intell. Robot. Syst.* 101 (1) (2021) 1–16.
- [19] C.A. Brochu, Phylogenetic approaches toward crocodylian history, *Annual Rev. Earth Planet. Sci.* 31 (2003) 357–397.
- [20] C.A. Brochu, Phylogenetics, taxonomy, and historical biogeography of alligatoroidea, *J. Vertebrate Paleontol.* 19 (sup002) (1999) 9–100.
- [21] C.S. Straub, Crocodiles; their natural history, folklore and conservation, 1973, pp. 404–405.
- [22] J. Harshman, C.J. Huddleston, J.P. Bollback, T.J. Parsons, M.J. Braun, True and false gharials: a nuclear gene phylogeny of crocodylia, *Syst. Biol.* 52 (3) (2003) 386–402.
- [23] G.J. Webb, S.C. Manolis, M.L. Brien, Saltwater crocodile *Crocodylus Porosus*. Crocodiles- status survey and conservation action plan, third ed., Darwin: Crocodile Specialist Group, 2010, pp. 99–113.
- [24] D. You-Zhong, W. Xiao-Ming, H.E. Li-Jun, et al., Study on the current population and habitat of the wild Chinese alligator, 9(2001), 2001, p. 102.
- [25] G. Grigg, C. Gans, Morphology and physiology of the crocodylia, *Fauna Australia* 2 (1993) 326–336.
- [26] F.E. Fish, Kinematics of undulatory swimming in the American alligator, *Copeia* 1984 (4) (1984) 839–843.
- [27] J.M. Hutton, Morphometrics and field estimation of the size of the Nile crocodile, *African J. Ecol.* 25 (4) (1987) 225–230.
- [28] A.L.A. Wiseman, P.J. Bishop, O.E. Demuth, et al., Musculoskeletal modelling of the Nile crocodile (*Crocodylus niloticus*) hindlimb: effects of limb posture on leverage during terrestrial locomotion, *J. Anatomy* 239 (2) (2021) 424–444.
- [29] J.S. Willey, A.R. Biknevicius, S.M. Reilly, K.D. Earls, The tale of the tail: limb function and locomotor mechanics in alligator mississippiensis, *J. Exp. Biol.* 207 (3) (2004) 553–563.
- [30] H.E.J. Veeger, F.C.T. van der Helm, Shoulder function: the perfect compromise between mobility and stability, *J. Biomech.* 40 (10) (2007) 2119–2129.
- [31] T. Wa, Foundations of Robotics: Analysis and Control, MIT Press, 1990.
- [32] H. Milton, The adaptive significance of tetrapod gait selection, *Am. Zool.* 20 (1) (1980).
- [33] R.J. Wassersug, Tetrapod gait patterns, *Science* 188 (4195) (1975) 1256–1258.